Title

THERMALLY ACTIVATED DISLOCATION GLIDE THROUGH A RANDOM ARRAY OF POINT OBSTACLES: NUMERICAL SIMULATION

Authors

Morris, J.W.
Klahn, Dale H.

Publication Date

1973-10-01

Submitted to Journal of Applied Physics

LBL-2276
Preprint c.1

THERMALLY ACTIVATED DISLOCATION GLIDE THROUGH A RANDOM ARRAY OF POINT OBSTACLES: NUMERICAL SIMULATION

J. W. Morris, Jr. and Dale H. Klahn

October 1973

Prepared for the U. S. Atomic Energy Commission
under Contract W-7405-ENG-48

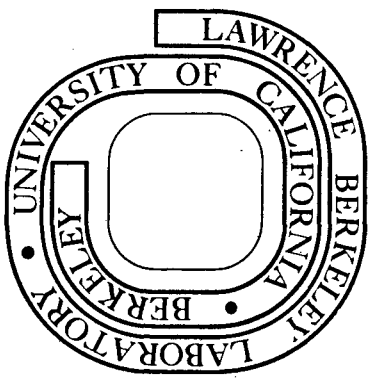

DISCLAIMER

LBL-2276

THERMALLY ACTIVATED DISLOCATION GLIDE THROUGH A RANDOM ARRAY OF POINT OBSTACLES: NUMERICAL SIMULATION

J. W. Morris, Jr. and Dale H. Klahn*
Department of Materials Science and Engineering
University of California, Berkeley and
Center for the Design of Alloys,
Inorganic Materials Research Division,
Lawrence Berkeley Laboratory

ABSTRACT

This paper reports results obtained from numerical simulation of the thermally-activated glide of an idealized dislocation through a random array of point obstacles. The array size is fixed at 999, and the dislocation-obstacle interaction is taken to have a simple step form. The variables governing glide are then the resolved shear stress, the temperature, and the obstacle strength, which may be phrased as dimensionless parameters. The principal subjects studied are three: (1) the stress required for athermal glide at given obstacle strength, and the characteristics of the obstacle configurations which determine this stress; (2) the glide path taken by the configuration, and the characteristics of the obstacle configurations encountered along this glide path; (3) the velocity of glide, and its dependence on the stress, the temperature, and the obstacle strength.

*Present Address: M-C 145
General Electric Company
175 Curtner Avenue
San Jose, California 95114

I. INTRODUCTION

As in the first paper of this series,[1] we are here concerned with the glide of a dislocation, idealized as a string of constant tension, through a random array of identical, immobile point obstacles. As discussed in the Introduction to reference 1, a proper description of thermally activated glide requires two types of information: the nature of the obstacle configurations encountered by the gliding dislocation and the proper statistics of thermal activation past these barrier configurations. In reference 1, we treated the statistics of thermal activation and discussed the statistical definition of the glide velocity. In the work reported here we have used numerical techniques to directly simulate thermally activated glide. The objectives of this work are three: (1) to characterize the obstacle configurations encountered along the glide path of a dislocation in sufficient details to provide guidance for theoretical work; (2) to check the validity of the approximations identified in reference 1; and (3) to study the velocity of glide as a function of applied stress, temperature, and obstacle strength, given a dislocation-obstacle interaction of simple "step" form.

The assumptions and basic equations used here are specializations of those used in reference 1. The glide plane of the dislocation is taken to be a square containing a random distribution of point obstacles, whose density is characterized by the area (a) per point or by the characteristic length $l_s = (a)^{1/2}$. The total area of the square array may be written in dimensionless form as the number of points contained: $A^* = A/a = n$. In the work reported here we studied arrays of fixed size, $n = 999$.

A dislocation in this plane is modelled as a flexible, extensible string of constant line tension, Γ, and Buergers vector, $\underset{\sim}{b}$, of magnitude b, taken to lie in the glide plane. The resolved shear stress τ impelling glide of this dislocation may be written in dimensionless form

$$\tau^* = \tau l_s b/2\Gamma \qquad (I.1)$$

Let the dislocation, under the applied stress τ^*, encounter a configuration of point obstacles denoted by (i) (figure 1). Between two adjacent obstacles the dislocation will take the form of a circular arc of dimensionless radius R^* ($=1/2\tau^*$). If the distance between any two adjacent obstacles along (i) exceeds $2R^*$ or if the dislocation line anywhere intersects itself then the configuration (i) is transparent to the dislocation and will be mechanically by-passed. If (i) is not transparent its mechanical stability is governed by the strength of the dislocation-obstacle interaction.

The obstacles are taken to be identical, circularly symmetric barriers to the dislocation whose effective range of interaction (d) is assumed small compared to their mean separation (l_s). They may hence be treated as point obstacles. At the $k^{\underline{th}}$ point obstacle along i the dislocation line forms the asymptotic angle ψ_i^k ($0 \leq \psi_i^k \leq \pi$). The force, F_i^k, which the dislcoation exerts on the $k^{\underline{th}}$ obstacle may be written in dimensionless form

$$\beta_i^k = F_i^k/2\Gamma = \cos(\psi_i^k/2), \qquad (I.2)$$

where $0 \leq \beta_i^k \leq 1$. The dislocation-obstacle interaction is given by a force-

displacement relation, $\beta(x/d)$, the effective dimensionless point force on the dislocation as it sweeps through the obstacle (ref. 2). In the work reported here the function $\beta(x/d)$ was assumed to have a simple step form (figure 2) with $\beta = \beta_c$ when $0 \leq x/d \leq 1$ and $\beta = 0$ otherwise. The force β_c measures the mechanical strength of the obstacle. A non-transparent line configuration of obstacles forms a mechanically stable barrier to the glide of a dislocation under stress τ^* if $\beta_i^k < \beta_c$ for all obstacles k on i.

If the configuration i is mechanically stable it must be passed by thermal activation. We ignore the possibility of thermally-activate bow-out between dislocations and require that the activation occur at an obstacle. The energetic barrier to thermal activation at the $k^{\underline{th}}$ obstacle on i is written

$$\left(\Delta G^{*k}_i\right)/kT = \alpha(\beta_c - \beta_i^k) \qquad \text{(I.3)}$$

where α is the "dimensionless reciprocal temperature"

$$\alpha = {}^{2\Gamma d}/_{kT} \qquad \text{(I.4)}$$

The residence time of the dislocation in configuration i is the time required for thermal activation past at least one obstacle point in i. The expected value of the residence time is (ref. 1, equation (24))

$$\langle t^* \rangle = \Lambda_i^{-1} \qquad \text{(I.5)}$$

where t* is dimensionless time, νt, with ν the mean frequency with which the dislocation attempts an obstacle, and Λ_i is the activation parameter

$$\Lambda_i = \sum_{k=1}^{N_i} \exp\left[-\alpha\left(\beta_c - \beta_i^k\right)\right] \tag{I.6}$$

where the summation is taken over the N_i obstacles on i. The variance of the residence time (σ_i^2) is (ref. 1, eq. (26))

$$\sigma_i^2 = \Lambda_i^{-2} \tag{I.7}$$

The probability that activation will occur first at the obstacle k on i is (ref. 1, eq. (28))

$$P(k,i) = (\Lambda_i)^{-1} \exp\left[-\alpha\left(\beta_c - \beta_i^k\right)\right] \tag{I.8}$$

To compute the glide velocity of the dislocation at given stress and temperature we assume that glide is controlled by thermal activation in the sense that the time required for dislocation glide between successive stable obstacle configurations is negligible compared to the time required for thermal activation past these configurations. If there are r stable dislocation configurations along a particular glide path χ through the array, then the expected transit time of a dislocation along χ is

$$\langle t^* \rangle = \sum_{i=1}^{r} (\Lambda_i)^{-1} \tag{I.9}$$

and its variance is

$$\sigma_\chi^2 = \sum_{i=1}^{r} (\Lambda_i)^{-2} \tag{I.10}$$

Given that the dislocation may take any one of many available glide paths through the array, the expected transit time is (ref. 1, equations 45, 46).

$$\langle t^* \rangle = \sum_{\chi} P_{\chi} \langle t^* \rangle \tag{I.11}$$

with variance

$$\sigma_{\chi}^2 = \sum_{\chi} P_{\chi} [\sigma_{\chi}^2 + (\langle t^* \rangle_{\chi} - \langle t^* \rangle)^2] \tag{I.12}$$

where P_{χ} is the probability that path χ is followed in a given trial. The velocity of glide is defined in a statistical sense only, but has the ergodic average

$$\langle v^* \rangle = n^{1/2} / \langle t^* \rangle \tag{I.13}$$

where v^* is the dimensionless area swept out by the dislocation per unit time divided by its projected length, the edge length of the array.

The determination of the velocity of glide through a random array of point obstacles is complicated since the available glide paths change with the applied stress, and the relative probabilities of these paths change with temperature. In reference 1 we identified approximations which appear useful when either α is large (low temperature) or the applied stress τ^* is very closed to the critical resolved shear stress τ_c^* for athermal glide through the array. These approximations were based on the observation that, given either large α or $\tau^* \sim \tau_c^*$ the dislocation will tend to follow the "minimum angle" path χ_o obtained under the constraint that the dislocation pass each configuration (i) by activating past the point k at which the angle ψ_i^k takes on its minimum value (or,

equivalently, at which β_i^k has its maximal value β_i). In the context of the present work these approximations take the following form. First, let α be so large that

$$\alpha >> {}^{\ln N_i}/_{\beta_i} - \beta_i^2 \tag{I.14}$$

for every configuration in χ_o, where β_i is the largest value of β_i^k and β_i^2 is the second largest value. Then equation I.13 becomes:

$$\langle v^* \rangle = n^{1/2} \left\{ \sum_{i=1}^{r_o} \exp\ [\alpha(\beta_c - \beta_i)] \right\}^{-1} \tag{I.15}$$

where the summation is taken over the r_o configurations in χ_o. If α satisfies the more stringent condition

$$\alpha >> {}^{\ln(r_o)}/_{\beta_2 - \beta_1} \tag{I.16}$$

where β_1 is the least of the β_i and β_2 is the next smallest,

$$\langle v^* \rangle = n^{1/2} \exp\ [-\alpha(\beta_c - \beta_1)] \tag{I.17}$$

and the glide velocity is determined by the time required for thermal activation at the weakest point along the strongest configuration in the array. Second, let τ^* be so near τ_c^* that the few stable barrier configurations of obstacles in the array are spatially separated in the sense that they have no obstacle points in common. Then the dislocation will follow path χ_o independent of temperature and

$$\langle v^* \rangle = n^{1/2} \left\{ \sum_{i=1}^{r_o} (\Lambda_i)^{-1} \right\}^{-1} \tag{I.18}$$

II. NUMERICAL SIMULATION

The central results given in the following sections were obtained through direct numerical simulation of dislocation glide. The code employed is based on an adaptation of a "circle-rolling" algorithm first used by Foreman and Makin[3]. The code models dislocation glide for given array size (n), applied stress (τ^*), obstacle strength (β_c), and reciprocal temperature (α).

Using a "pseudo-random number generator", available as a computer subroutine, the code first distributes a given number (n) of points over a square which represents the glide plane. It then lays mirror image boundary conditions. The points are identical, and are given a specified obstacle strength β_c. Given the array and the applied stress, τ^*, which fixes the radius (R*) of dislocation bow-out between obstacle points, the initial dislocation position is obtained using an analytical equivalent of the following procedure.

(1) A circle of dimensionless radius (R*) is moved up the left hand boundary of the square glide plane until it makes contact with an obstacle in the array. The circle center remains on the left boundary, assuring satisfaction of the mirror image boundary condition. The arc of the circle from the left boundary to the obstacle defines the first segment of the dislocation line. This dislocation line impinges normally on the boundary: in this sense the mirror image boundary is equivalent to a free surface.

(2) A circle is then rotated counter-clockwise about the obstacle until a second obstacle of the array is contacted. The arc of this

circle between the first and second obstacles defines the second segment of the dislocation. The force (β_1) on the first obstacle is easily related algebraically to the distance between the centers of the circles defining the first and second dislocation segments. If β_1 is less than β_c, obstacle 1 is a mechanically stable barrier to the dislocation. A circle is then rotated counter-clockwise about obstacle (2) until it contacts an obstacle (3) of the array. The arc of this circle between obstacles (2) and (3) defines the third segment of the dislocation line, and the distance of the center of this circle from the center of the circle connecting obstacles (1) and (2) is used to compute the force β_i^2 on obstacle (2).

The dislocation line is extended by successive circle rollings until the opposite end of the array is reached or until a point (k) is reached such that circle rolling about (k) does not find a point of the array giving $\beta_i^k \leq \beta_c$. In the latter case the point (k) is erased from the array (equivalently, it is mechanically by-passed by the dislocation). The code returns to point (k-1) and attempts to find a new extension of the dislocation line by circle rolling about this point. When a line is found such that the two sides of the array are connected via a configuration of obstacles (i) with $\beta_i^k < \beta_c$ for all k on i, this line is recognized to be the first stable configuration of the dislocation. The mirror boundary condition on the right hand side of the array ensures that the dislocation impinges normally on the right hand boundary.

(3) Given a stable line configuration the code may compute and tabulate interesting properties of the configuration, such as the forces

$\{\beta_i^k\}$, the distribution of dislocation segment lengths, and the activation parameter Λ_i for a particular value of the temperature parameter α. The code then breaks this configuration by erasing a selected point (k) (equivalently, letting the dislocation thermally activate past obstacle (k,i)), and finds the $(i+1)^{\underline{th}}$ mechanically stable configuration by repeating the circle-rolling process, starting with obstacle (k-1).

In practice, we select the activation point (k) in one of two ways. To generate a statistically chosen glide path, χ, the code first computes the activation probabilities P(k,i) from the β_i^k and α by equation (I.8), then calls a random number to select the obstacle actually passed according to the P(k, i). To generate the "minimum angle" path χ_o the code constrains the activation event to the point (k, i) at which β_i^k takes on its maximum value β_i. The residence time in configuration (i) is stochastically independent of the activation site and may be computed according to the equations given in Section I and discussed in reference 1.

(4) Successive stable dislocation configurations are identified, and the time of passage computed by repeating steps (1) - (3) above. In the work reported here, glide was terminated when any part of the dislocation touched the upper boundary of the glide plane. The expected transit time, its scatter, and the ergodic average of the glide velocity are then computed from the relations given in Section I.

The code described above has two shortcomings which should be noted, though they do not sensibly affect the results given in the following sections. First, a gliding dislocation may fold around a group of closely spaced obstacles and, by closing on itself, leave an isolated

dislocation loop. Only certain of these loops are found with a "circle-rolling" algorithm. However, as Kocks[4] found, and our observations confirm, this looping becomes important only when τ^* and β_c are large. Moreover, excepting the limit of τ^* near 0.8 and β_c near 1.0, the loops formed at stresses below the critical resolved shear stress (τ_c^*) are mechanically weak relative to the stable dislocation configurations and collapse through thermal activation in times short compared to the expected transit time. Hence, they do not affect the average glide velocity. Second, while the dislocation line is mechanically unstable if it anywhere intersects itself, self-intersections are found by the code only when they occur at an obstacle point. However, specific observation of the stable dislocation lines show that intersections other than at obstacle points are very rare unless τ^* and β_c are large, and almost invariably occur in weak configurations which contribute negligibly to the glide velocity[5].

III. MECHANICAL PROPERTIES: THE CRITICAL RESOLVED SHEAR STRESS

A central mechanical property of a glide plane containing a random distribution of point obstacles is the critical resolved shear stress (τ_c^*) at which a dislocation can cross the glide plane without benefit of thermal activation. Much of the prior work on glide through random arrays of point obstacles has been devoted to the problem of finding (τ_c^*) as a function of the "obstacle strength" (β_c). This prior work includes both numerical simulation[3, 4] and analytic studies [6,8].

1. The critical resolved shear stress

The available data comes from numerical simulations by Kocks[4] and by Foreman and Makin[3]. Kocks used a graphical technique to estimate τ_c^* for "uncuttable" obstacles ($\beta_c = 1.0$) in an array of 550 point obstacles. He found $\tau_c^* \simeq 0.8$. Foreman and Makin[2] used a computer code similar to that described in Section II to conduct a comprehensive study of τ_c^* over the full range of obstacle strengths ($0 \leq \beta_c \leq 1.0$) for arrays containing from 10^3 to 10^4 points. Their data, which confirms Kock's estimate in the limit $\beta_c = 1.0$, is compared with results of the present study in Figure 3.

In the present work we adopted a variant of the procedure of Foreman and Makin[2] which fits more naturally in a study of thermally activated glide. By fixing a stress (τ^*), arbitrarily setting β_c at 1.0, letting the dislocation move through the array along the minimun angle path χ_o, and measuring the maximum force (β_i) for each obstacle configuration encountered, we may determine the maximum force (β_1) which the dislocation exerts on the most stable obstacle configuration opposing glide at stress τ^*. This value (β_1) is the minimum value the obstacle

strength (β_c) may have if the obstacle array is to be mechanically stable with respect to glide. Hence if $\beta_c = \beta_1$, $\tau_c^* = \tau^*$. Since it may be easily shown that β_1 is a monotonically increasing function of τ^* in a given array, a determination of β_1 as a function of τ^* is equivalent to a measure of τ_c^* as a function of β_c.

The strength β_1 is plotted as a function of the applied stress τ^* in figure 3. The bars indicate the range of values obtained in tests of several arrays. At the higher stresses not all arrays contain non-transparent configurations. Six of 20 arrays tested at $\tau^* = 0.75$ were transparent; 92 of 100 arrays tested at $\tau^* = 0.85$ were transparent. The solid line in the figure is a schematic representation of the data obtained by Foreman and Makin[3]. The dashed line is a plot of the "Friedel relation"[9]

$$\beta_c = (\tau^*_c)^{2/3} \qquad \text{(III.1)}$$

To indicate the nature of the scatter in data obtained at given stress, the insert in the figure shows normalized histograms of the β_1 values found in tests of the same 20 arrays at three stresses, $\tau^* = 0.1$, 0.3, and 0.5.

The results obtained generally confirm those of Foreman and Makin. At low stresses the Friedel relation, equation (III.1) is a good approximation. The limiting stress at which one half the arrays become transparent is near 0.8.

Our results also show an appreciable scatter in the strengths of arrays containing approximately 10^3 points. This scatter should decrease as the number of points in the array is increased, but may, nonetheless,

have significant mechanical consequences. Consider, for example, an idealized crystal made up of parallel glide planes each of which contains approximately 10^3 obstacles strength $\beta_c = 1.0$. Let the crystal contain sources of non-interacting dislocations on each glide plane. Near zero temperature the average glide plane will yield at a value of τ^* near 0.8; however, the crystal may undergo substantial plastic deformation through glide on well-defined slip planes at $\tau^*=0.75$.

2. Characteristics of the strength-determining configurations

As has been pointed out, the strength-determining obstacle configuration in a given array at given stress is that configuration along the glide path of the dislocation for which the maximum force exerted by the dislocation (β_i) takes on it minimum value (β_1). These strength-determining configurations are of central importance to dislocation glide since they not only determine τ_c^* but, as we shall show in the following sections, also have a dominant influence on the velocity of thermally activated glide over a wide range of conditions.

In the current literature the strength-determining configurations are often discussed using the simple model proposed by Friedel.[9] Friedel assumed that when τ^* is small the obstacle configurations encountered will approximate straight lines of equispaced points. Using the condition that the average dimensionless area swept per point cut by the dislocation be one, he found equation III.3 for the force exerted by the dislocation on each obstacle and the additional relation,

$$1^* = (l/l_s) = (\tau^*)^{-1/3} \qquad \text{(III.2)}$$

giving the separation between obstacles along the dislocation line. While this model was proposed to treat thermally activated glide at high temperature, its adaptation by Fleisher and Hibbard[8] and the subsequent demonstration by Foreman and Makin[3] that equation III.1 is a good approximation over a wide range of τ^* values led to its use in discussing the strength determining configurations. Thus Foreman and Makin[3] used the accuracy of equation III.1 at small τ^* to infer the validity of both the Friedel picture of the dislocation and the relation (III.2) for the mean obstacle spacing ($\bar{l}^*$) in the strength-determining configuration. Their assumptions have been followed in more recent work.

More detailed analyses of the obstacle configurations opposing glide have been published by Kocks[6] and by Labusch[10]. However, since both considered the obstacle configuration along a randomly placed dislocation their results are not directly applicable to the strength-determining configurations.

Given this background we conducted a numerical analysis of the characteristics of strong obstacle configurations, including their overall shapes, the distribution of forces (β_i^k), and the mean and distribution of the distance between obstacles (l^*).

The overall shapes of the strong configurations are illustrated in the example of figure 4 which shows the strongest configurations found in glide through a typical 999 point array at three stresses: $\tau^* = 0.1$, 0.3, and 0.5. The three configurations are essentially independent of one another. Their shapes change roughly as expected; the strength-determining configuration becomes more irregular as the dimensionless stress

is raised. However, at $\tau^* = 0.1$, which is well within the range in which equation III.1 yields a good approximation, the dislocation line remains irregular. The results shown in figure 4 are typical of those obtained in tests using a number of arrays.

To study the distribution of forces along strong configurations, we compiled and compared the $\{\beta_i^k\}$ for the strongest configurations in several arrays at given values of τ^*. The comparision showed that if histograms of the β-values were made using the variable (β/β_i) the histograms were similar both for the strongest configurations in different arrays and for the strongest configurations at different stresses. To find the general form of these histograms we used the following procedure. For given τ^* we chose β_m such that virtually all 999 point arrays would contain configurations having $\beta_i \leq \beta_m$, but also such that $\beta_m - \beta_1$ would be small. We then found one configuration with $\beta_i \sim \beta_m$ in each of a number of arrays at given τ^*, compiled the $\{\beta_i^k\}$ for each of these configurations, and used this compilation to establish the normalized density $n(\beta/\beta_m)$.

The results are plotted in figure 5, which shows the normalized density $n(\beta/\beta_m)$ at three stresses, $\tau^* = 0.1$ (100 arrays, $\beta_m = 0.2339$), $\tau^* = 0.3$ (100 arrays, $\beta_m = 0.5080$), and $\tau^* = 0.5$ (20 arrays, $\beta_m = 0.7109$). The normalized density functions at the three stresses are nearly coincident. The slight drop in $n(\beta/\beta_m)$ near 1.0 is spurious; the configurations used in this compilation have a distribution of strengths $\beta_i \sim \beta_m$. Direct comparision with the histograms of (β/β_m) for the strength-determining configurations in individual arrays shows general agreement. The scatter between single-configuration histograms is, however, large, as is expected given the small number of obstacles on a typical strength-deter-

mining configuration in a 999-point array (N~21 at $\tau^* = 0.1$, 34 at $\tau^* = 0.3$, 52 at $\tau^* = 0.5$).

Two points of theoretical significance may be drawn from figure 5. First, the similarity of the density functions $n(\beta/\beta_m)$ suggests the existence of a stress-independent density function which governs the distribution of the forces (β_i^k) on strong configurations. This limiting density function need not necessarily be of the form $n(\beta/\beta_m)$. If the data in figure 5 are replotted in terms of the angles ψ_i^k as $n(\psi/\psi_m)$, the agreement is essentially as good over the range of stresses tested. Second, although equation (III.1) is well obeyed when τ^* is small, there is no apparent tendency for $n(\beta/\beta_m)$ to approach the limiting distribution of the Friedel model:

$$n(\beta/\beta_m) = \delta\left\{\beta/\beta_m - (\tau^*)^{2/3}/\beta_m\right\} \qquad \text{(III.3)}$$

where δ is the Dirac δ-function.

To examine the mean and distribution of l^* we formed histograms of the l^* values along individual strength-determining configurations and also found normalized density functions by compiling the l^* values along the configurations used to obtain figure 5. The resulting density functions cannot easily be set in stress-independent form. Their mean values, $\bar{l}^*$, are plotted in figure 6 against the predictions of the Friedel relation III.2. For completeness we have included the $\bar{l}^*$ estimates of Labusch[10] and Kocks[6]; the Labusch estimate is virtually identical to that of Friedel.[9] The points on the "experimental" curve in figure 6 are the $\bar{l}^*$ values determined from the normalized density functions. The bars give the range of $\bar{l}^*$ for the strongest configurations in twenty arrays.

As is apparent from figure 6, the Friedel equation (III.2) seriously overestimates $\bar{l}^*$ over the range of stresses studied. The discrepancy increases as τ^* becomes small, a trend opposite to that which would be observed if the validity of equation III.1 implied the validity of the Friedel model of the dislocation line.

IV. OBSTACLE CONFIGURATIONS ENCOUNTERED ALONG THE GLIDE PATH

As discussed in reference (1) the path followed by a dislocation in glide at finite temperature is statistically determined. The glide path is well defined only in limiting cases, three of which were identified. First, when the temperature is sufficiently high the parameter α is so small that all activation events are almost equally likely. The successive configurations encountered by the dislocation will then be random in the sense that they are determined from the initial configuration through a random sequence of activation events. Second, when the temperature is sufficiently low α is so large that (in a finite array) activation is almost certain to occur at the point along the configuration where the applied force β_i^k has its maximum value β_i (or the angle ψ_i^k has its minimum value ψ_i). The dislocation will then follow the minimum angle path, χ_o. Third, when the stress τ^* is very near τ_c^* the stable obstacle configurations are spatially separated from one another in the sense that they have no obstacle points in common. The path followed by the dislocation is then independent of the statistics of thermal activation. The configurations encountered necessarily lie along the minimum angle path (χ_o).

The work reported here focused on glide at moderate to large values of the dimensionless reciprocal temperature, α. The glide paths are then closely related to the "minimum angle" path, χ_o.

1. Characteristics of the path χ_o.

Three characteristics of the path χ_o were studied. (1) the distribution of mechanical strengths (β_i) of the obstacle configurations en-

countered along χ_o as a function of the stress τ^*; (2) the distribution of forces (β_i^k) along configurations in χ_o as a function of τ^* and β_i; (3) the spatial distribution of the strong configurations (β_i near β_1) in χ_o. The distribution of the β_i determines the fraction of the non-transparent configurations which are mechanically stable at a given obstacle strength (β_c) and determines the velocity of glide at given α in the minimum angle approximation. The distribution of the β_i^k determines the true values of the activation parameter Λ_i at given α. The spatial distribution of the strong configurations determines the value of the obstacle strength β_c at which the high stress limit is reached in an array at given τ^*. The spatial distribution of strong configurations influences both the "jerkiness" of dislocation glide at low temperature and the tendency of the dislocation to adhere to the path χ_o during glide at finite temperature.

The distribution of the β_i along χ_o was studied as a function of τ^* by compiling the strengths of all lines encountered along the minimum angle path in twenty arrays each containing 999 points. Typical results are shown in figure 7, where we have plotted the density (per array) of configurations of strength β_i encountered along χ_o at stress $\tau^* = 0.1$, 0.3, and 0.5. The area under these curves gives the total number of non-transparent configurations (r per array) along χ_o at given stress, and is $r = 890$ at $\tau^* = 0.1$, $r = 750$ at $\tau^* = 0.3$, and $r = 470$ at $\tau^* = 0.5$. Given an obstacle strength, β_c, the expected number of mechanically stable configurations at τ^* is simply the area under the appropriate curve over the range $\beta \leq \beta_c$.

The shape of the distribution of β_i along the minimum angle path in a particular 999 point array at applied stress τ^* corresponds closely to the shape of the composite distribution function. The principal variation from one array to the next is in the distribution of strengths near β_1, and is associated with the variation in β_1 values discussed in the previous section.

The β_i - distribution is strongly influenced by the applied stress (τ^*). As is apparent from figure 7, increasing τ^* increases the minimum, β_1, decreases the number of non-transparent configurations encountered in glide through the array, and alters the shape of the distribution.

The distribution of forces, $\{\beta_i^k\}$, along a configuration in χ_o is, to a reasonable approximation, determined by the strength β_i. When $\beta_i \sim \beta_1$ the β_i^k are distributed according to the functions described in the previous section. Even when β_i is appreciably larger than β_1 the distribution of the β_i^k is still dominated by this "strong-line" distribution. This latter result follows from the way in which the path χ_o is generated. In each step along χ_o the dislocation activates past the obstacle at which the maximum force, β_i, is applied, and hence always eliminates the maximum, β_i, from the set of applied forces $\{\beta_i^k\}$. Excepting the first few configurations encountered as the dislocation moves into the array, the distribution of the β_i^k always approximates the strong-line distribution for $\beta \leq \beta_1$, and will also include one or a few $\beta > \beta_1$ scattered over the range $\beta_1 < \beta \leq \beta_t$. This character of the distribution is illustrated in figure 8, which shows a normalized distribution obtained by compiling all angles along the $50^{\underline{th}}$ configuration encountered along the path χ_o in 200 arrays at $\tau^* = 0.1$. As can be seen by comparing this figure with

figure 6, the strong line distribution is well obeyed for $\beta \tilde{<} 0.22$, which is close to β_1 for this stress. The distribution also includes a scattering of larger β- values, reflecting the distribution of the strengths, β_i, of the lines used to compose this histogram. This and more detailed studies of the character of individual configurations show that the distribution of $\{\beta_i^k\}$ along a line of given β_i in χ_o may be roughly approximated by taking the strong-line distribution for $\beta \leq \beta_o$, and adding one point at $\beta = \beta_i$.

The third property of the path χ_o studied in this investigation was the spatial distribution of the strong obstacle configurations. The principal observation from this study is the tendency of the strong configurations to bunch so that they share many obstacle points in common. Figure 9 illustrates the five strongest configurations encountered in glide along χ_o through a typical array at $\tau^* = 0.1$. Four of these five configurations nearly superimpose. The superposition of the strong configurations has the consequence that the "high stress" limit is only reached when τ^* is very close to τ_c^*; in the array shown τ^* must be so near τ_c^* that only one configuration remains stable. This result is typical of 999 point arrays at all stresses studied.

2. The glide path at finite temperature

As the temperature is raised from near zero the parameter α decreases and the path, χ, followed in glide becomes a stochastic sequence different from χ_o. It is difficult to characterize these finite temperature paths. However, one can make the general statement that a stochastic path χ will tend to contain fewer strong configurations than the minimum angle path

χ_o, and hence will permit somewhat faster dislocation glide. This conclusion follows for two reasons. First, all spatially independent strong configurations are necessarily contained in the sequence χ_o, but do not necessarily appear in a stochastically determined glide sequence. Second, the strongest configuration in any cluster of strong configurations is necessarily contained in χ_o. Not only may this strongest configuration be excluded from a stochastically determined glide path, but if activation happens to occur at an obstacle common to several strong configurations of the cluster, a sequence of strong configurations may be excluded.

Even in a 999 point array the actual glide path (χ) begins to deviate noticeably from χ_o at rather large values of the parameter α. The reason is apparent from the distribution functions presented above. The distribution of forces $\{\beta_i^k\}$ along a strong line is such that (Fig. 5) there is a high density of β values near β_i. Hence the difference between the largest and next-largest of the β_i^k tends to be small. The right hand side of the inequality (I.14) which determines the low temperature limit is then large, and the minimum angle approximation fails unless α is correspondingly large. For example, the strongest configuration in the array shown in figure 9 at $\tau^* = 0.1$ has $\beta_1 = 0.2154$, $\beta_1^2 = 0.2113$, and $N_i = 21$. The condition (I.14) then requires $\alpha >> 750$ for the low temperature limit in this configuration. The value of the right-hand side of equation (I.14) is, to a rough approximation, independent of stress; $\alpha >> 750$ is a typical condition for the minimum angle approximation for a strong line.

V. THE GLIDE VELOCITY

The numerical studies of glide velocity reported in this section focus on three problems: (1) the statistics of glide at finite temperature and the accuracy of the "minimum angle" and "minimal sequence" approximations; (2) the dependence of glide velocity on the parameters α, τ^*, and β_c (i.e., on temperature, stress, and obstacle strength) given the assumptions discussed in Section I; (3) the superposition of independent glide in distinct arrays and implications for the deformation of model crystals.

1. Statistics of glide

The results of a typical simulation at finite temperature are shown in figure 10, where we have plotted the dimensionless velocity v^* (specifically, its negative logarithm) against the thermal parameter α for a particular 999 point array of obstacles with strength $\beta_c = 0.63$. Data are shown for two stresses: $\tau^* = 0.1$, which is approximately 0.2 of the critical resolved shear stress at this obstacle strength, and $\tau^* = 0.4$, which is approximately 0.8 of τ_c^*. The stochastic velocity curves were found by allowing six independent passages through the array at each condition for which a data point is shown. The mean transit time, $\langle t^* \rangle$, and its variance, σ^2, were computed from the results of the individual trials according to equations (I.11) and (I.12). The expected values, $\langle v^* \rangle$, of the dimensionless glide velocity were then obtained from equation (I.13). The results are shown as circles in the figure. The bars indicate the variation of velocity as the transit time ranges over the interval $\langle t^* \rangle \pm \sqrt{\sigma^2}$. The numerical results found with $\tau^* = 0.4$ are tabulated in Table 1.

The results obtained from this unrestricted simulation are compared to estimates derived from three approximations. The bases of these approximations are discussed in Section I. The first is the minimum angle approximation, in which we assume that the dislocation follows the path χ_o and passes each configuration encountered at the point at which the angle ψ is minimum, giving β its maximum value β_i. In this case,

$$\langle t^* \rangle = \sum_{i=1}^{r_o} \exp \{\alpha(\beta_c - \beta_i)\} \qquad \text{(III.1)}$$

and

$$\sigma^2 = \sum_{i=1}^{r_o} \exp \{2\alpha(\beta_c - \beta_i)\} \qquad \text{(III.2)}$$

where r_o is the number of stable configurations along the glide path χ_o. The second estimate is obtained from the minimum angle approximation under the additional constraint that only the strongest configuration is considered; $\langle t^* \rangle$ is set equal to the expected time to activate past the strongest configuration encountered (where β_i takes its minimum value β_1) at its minimum angle point. In this case $\langle t^* \rangle$ is given by the Arrenhius equation

$$\langle t^* \rangle = \exp \{\alpha(\beta_c - \beta_1)\} \qquad \text{(III.3)}$$

and

$$\sigma^2 = \langle t^* \rangle^2 \qquad \text{(III.4)}$$

The third estimate employs the minimal sequence approximation, in which we assume that the dislocation follows the glide path χ_o, but passes each configuration at a stochastically chosen point. In this case

$$\langle t^* \rangle = \sum_{i=1}^{r_o} (\Lambda_i)^{-1} \qquad \text{(III.5)}$$

and

$$\sigma^2 = \sum_{i=1}^{r_o} (\Lambda_i)^{-2} \qquad \text{(III.6)}$$

where Λ_i is the activation parameter for the i^{th} configuration and is given by equation (I.6).

As is apparent from figure 10 and Table I all three approaches give a generally reasonable estimate of the velocity of glide through this array when α is greater than 100. As is expected from the underlying assumptions, the full minimum angle approximation underestimates $\langle v^* \rangle$ and slightly exaggerates the upward concavity in the curves of $[-\ln\langle v^* \rangle]$ vs. α. An Arrenhius equation based on activation at the minimum angle in the strongest configuration encountered overestimates $\langle v^* \rangle$ and misses the slight upward concavity of the curves. The minimal sequence approximation yields a particularly good fit over the range of α studied.

The success of these approximations argues for their utility in estimating the glide velocity, but should not be taken to infer the accuracy of the assumptions on which they are based. For example, a detailed analysis of the numerical simulation at $\tau^* = 0.4$ showed that the path χ_o contained 30 stable configurations. These overlapped significantly; in fact, the four most stable configurations were almost coincident. While the dislocation tended to follow the path χ_o during glide there were significant deviations. In particular, the strongest configuration lay on the actual glide path in only a minority of the trials (2 of 6 at α = 400 and α = 300, 3 of 6 at α = 200). Both the overlap of strong configu-

rations and the deviation from χ_o violate the assumptions on which the minimal sequence approximation is based. Its success should rather be taken as evidence that the ergodic average of the glide paths actually followed by the dislocation is sufficiently like the path χ_o to be represented by it. This point is documented in figure 11, in which we compare the cumulative distribution of the activation parameter Λ along the path χ_o at $\alpha = 300$ to the corresponding distribution for the weighted average of the statistically-chosen paths taken in six independent trials at the same value of α. The merit of χ_o as a representative path is also largely responsible for the reasonable accuracy of the minimal angle approximations over this range α.

The results presented here are fairly typical of those obtained from simulation of glide in a number of arrays over the range of τ^* studied, 0.05 to 0.6. The minimal sequence approximation provides a good estimate of $\langle v^* \rangle$ when α is greater than about 50. The miminum angle approximation yields a reasonable, though less accurate, approximation when α is greater than about 100. However, the good fit obtained in the present case ($\tau^* = 0.4$) with an Arrenhius equation based on activation at the minimum angle in the strongest configuration is somewhat atypical, and must be attributed to the mutual cancellation of significant errors. This Arrenhius equation is always useful, but is generally less precise than shown here when $\alpha<400$.

2. The influence of temperature, stress and obstacle strength

Given the accuracy of the minimal sequence approximation, illustrated in the previous section, we use it as the basis of a discussion of the

dependence of the glide velocity $\langle v^* \rangle$ on the parameters α, τ^*, and β_c, or equivalently, on the temperature, stress and obstacle strength. From equations (I.18) and (I.6) the expected value of the transit time $\langle t^* \rangle$ alond the path χ_o, which is the estimated in the minimal sequence approximation, may be written

$$\langle t^* \rangle = \left\{ 1 + (Q-T_1) + R \right\} \exp[\alpha(\beta_c-\beta_1)] \tag{V.1}$$

where the strongest obstacle configuration along χ_o is labelled $i = 1$. The symbols Q, T_i, and R denote the series:

$$Q = \sum_{i=2}^{r_o} \exp\,[-\alpha(\beta_i-\beta_1)] \tag{V.2}$$

$$T_i = 1 - \left\{ 1 + \sum_{k=2}^{N_i} \exp\,[-\alpha(\beta_i-\beta_i^k)] \right\}^{-1} \tag{V.3}$$

and

$$R = \sum_{i=2}^{r_o} T_i \exp\,[-\alpha(\beta_i-\beta_1)] \tag{V.4}$$

where r_o is the number of stable configurations along the path χ_o, β_i is the largest value of β in the $i^{\underline{th}}$ configuration, and N_i is the number of obstacles in the $i^{\underline{th}}$ configuration. The series Q, T_i, and R all decrease as α increases. $\langle t^* \rangle$ has the asymptotic form

$$\langle t^* \rangle \tilde{=} \left\{ 1 + (Q-T_1) \right\} \exp\,[\alpha(\beta_c-\beta_i)] \tag{V.5}$$

where

$$T_1 = \sum_{k=2}^{N_i} \exp\,[-\alpha(\beta_1-\beta_i^k)] \tag{V.6}$$

and Q is given by equation (V.2). Hence the glide velocity $\langle v^* \rangle$ has the asymptotic form

$$\langle v^* \rangle = n^{1/2} [1-(Q-T_1)] \exp [-\alpha(\beta_c-\beta_1)] \qquad (V.7)$$

The series Q is the lead correction term giving the decrement in $\langle v^* \rangle$ due to the fact that the dislocation must activate past stable configurations in addition to the strongest along χ_o. The series T_1 is the lead correction term giving the increment to $\langle v^* \rangle$ from the possibility of thermal activation at a point other than the weakest in a stable configuration. The parameter T_1 specifically measures this effect for the strongest configuration (i=1). Equation V.7 differs from that obtained using the minimum angle approximation through the inclusion of T_1.

Equation V.7 can be developed quantitatively using results given in the preceeding sections. The strength β_1 can be estimated from the stress τ^* according to the relation illustrated in figure (3), and given α and β_1 the series T_1 and Q may be approximated from the histograms illustrated in figures (5) and (7). We shall present this quantitative development in a future publication; a qualitative discussion fulfills the purpose of the present paper.

(a) The effect of temperature

It follows from equation V.7 that when α is arbitrarily large $\langle v^* \rangle$ if given by the Arrenhius equation

$$\langle v^* \rangle = n^{1/2} \exp [-\alpha(\beta_c-\beta_1)] \qquad (V.8)$$

As α decreases (temperature increases) the parameters Q and T_1 become significant, and $\langle v^* \rangle$ deviates from equation (V.8). The direction of the deviation is determined by the relative magnitudes of Q and T_1. For the numerical studies we have conducted, which treat 999 point arrays and

cover roughly the range $\alpha \gtrsim 50$, $0.05 \leq \tau^* \leq 0.6$, and β_c such that $\tau^* \leq 0.8\tau^*_c$, the series Q tends to dominate and $\langle v^* \rangle$ deviates from the Arrenhius equation to the negative side by an amount which increases as α decreases. This behavior is illustrated in figure (10). It should, however, be apparent that as $\tau^* \to \tau^*_c$ an opposite trend will be observed: T_1 will dominate and $\langle v^* \rangle$ will deviate in the positive sense from the Arrenhius equation V.8. This latter behavior is obvious in the limit, since when τ^* is sufficienly close to τ^*_c the array contains only one stable line and Q is identically zero.

As we have emphasized elsewhere[11] the temperature affects the character of glide as well as its velocity. As the temperature is decreased (at fixed τ^* and β_c) the dislocation spends an increasing fraction of its total transit time in the few strongest configurations, with the result that glide is increasingly "jerky". This behavior is again obvious in the limits, since as $\alpha \to \infty$ the mean residence time in the strongest configuration becomes arbitrarily larger than the mean residence time in any other configuration, while as $\alpha \to 0$ the mean residence times in all configurations are comparable.

(b) The effect of stress

The effect of the applied stress, τ^*, may also be discussed in terms of its influence on equation V.7. Its dominant influence is through the strength, β_1, which varies according to the relation $\beta_1(\tau^*)$ plotted in figure (3) and discussed in the accompanying text. As τ^* increases, β_1 increases, which in turn causes an exponential increase in the glide velocity $\langle v^* \rangle$. The applied stress, τ^*, also influences the pre-exponential term in equation V.7, though in a less striking way. The value of Q tends

to decrease as τ^* increases, while the value of T_1 remains roughly the same. Hence the increase in $\langle v^* \rangle$ with τ^* tends to be greater than one would predict on the basis of the Arrenhius equation, V.8. Moreover the deviation of equation V.7 from a simple Arrenhius form becomes less pronounced as τ^* increases, and may change in sign. The former effect is apparent in the velocity curves shown in figure (10); the data at $\tau^* = 0.4$ are fit more closely by equation V.8 than are those at $\tau^* = 0.1$.

The decrease in Q with increasing τ^* has two sources. First, as τ^* increases the histogram of β_1 values along χ_o (figure (7)) flattens so that there tend to be fewer configurations having β_i near β_1. The series determining Q then has fewer terms of significant magnitude, and its sum decreases. Second, as τ^* increases the histogram is shifted along the β-axis, so that there are fewer stable configurations along χ_o and the total number of terms in the series determining Q decreases. However, when α is reasonably large this latter effect is important only if τ^* is near τ_c^*; otherwise the terms deleted from the series have negligible magnitude.

As we have emphasized elsewhere[10], an increase in τ^* tends to cause the glide to become more "jerky". Excepting the cast $\tau^* \approx \tau^*_c$ this phenomenon is due to the flattening of the β_i histogram with increasing τ^* (figure (7)). The applied stress is, however, less important than the temperature in determining the "jerkiness" of dislocation glide.

(c) The effect of obstacle strength

The obstacle strength (β_c) appears explicitly in the exponential in equation V.7. A change in β_c at fixed τ^* will cause the velocity

$\langle v^* \rangle$ to undergo an exponential change in the opposite direction. In general the pre-exponential in equation V.7 is unaffected by a change in β_c. The series T_1 is independent of β_c. The value of Q will be affected only if β_c is so close to β_1 ($\tau^* \sim \tau^*_c$) that a change in obstacle strength causes terms of significant magnitude to be added to or deleted from the series determining Q.

3. Deformation of an idealized crystal

In reference (1) we discussed how the results of this investigation can be used to model steady-state deformation of an idealized crystal made up of parallel glide planes. The steady-state strain rate of such a crystal can be computed if characteristics of the mobile dislocation density are known, and if the dislocations are assumed independent of one another. Two limiting distributions of mobile dislocations were identified. In the first we assumed a constant density of non-interacting, mobile dislocations ergodically distributed through the whole crystal. In this case the average glide velocity (v^*) is given by

$$\bar{v}^* = n^{1/2}/\bar{t}^* \qquad \text{(V.9)}$$

where

$$t^* = \frac{1}{S} \sum_{l=1}^{S} \langle t^* \rangle_l \qquad \text{(V.10)}$$

is the average of the expected transit times in a crystal containing S glide planes. As a second limiting case, we assumed a distribution of mobile, non-interacting dislocations which is uniform in the sense that the time average of the density of dislocations on each glide plane is the same. In this case the average glide velocity ($\tilde{v}^*$) is the simple

average of the expected glide velocity on the planes composing the crystal:

$$\tilde{v}^* = \frac{1}{S}\sum_{l=1}^{S} \langle v^* \rangle_l = \frac{n^{1/2}}{S}\sum_{l=1}^{S} \langle t^* \rangle_l^{-1} \qquad (V.11)$$

It should be apparent from equations (V.9 - V.11) that if $\langle v^* \rangle$ varies from plane to plane these two dislocations distributions will yield different values for the overall average glide velocity. The velocity $\bar{v}^*$ is principally influenced by glide on those planes on which the transit time $\langle t^* \rangle$ is largest, or those on which glide is most difficult. The velocity $\tilde{v}^*$ is principally influenced by glide on those planes on which the expected velocity $\langle v^* \rangle$ is largest, or those on which glide is easiest. Moreover, if $\langle v^* \rangle$ varies from plane to plane the two distributions will lead to qualitatively different types of crystal deformation. With an ergodic distribution of mobile dislocations all glides planes will be active and the overall deformation of the crystal will be evenly distributed among them. With a uniform distribution of mobile dislocations the deformation will be concentrated on a few well-defined planes, those on which glide is easiest.

The points made above may be illustrated with a simple example. Let a hypothetical crystal contain four parallel glide planes, which we specify by randomly selecting four arrays of 999 points, and let the obstacles impeding glide through these planes have strength $\beta_c = 0.63$. The glide characteristics of these planes are shown in figure (12), where we have plotted the glide velocity $\langle v^* \rangle$ as a function of the thermal parameter, α, for each plane at each of the four stresses, $\tau^* = 0.1, 0.2, 0.3$ and 0.4.

As shown in the figure, at $\tau^* = 0.1$ and 0.2 the velocity of glide is essentially the same in the four planes, while at $\tau^* = 0.3$ and $\tau^* = 0.4$ the velocities scatter by an amount which increases with α. The increasing spread in $\langle v^* \rangle$ as τ^* is raised is in large part attributable to the increasing spread in the β_1 values as τ^* is raised, a behavior illustrated in the insert to figure (3).

At stresses of $\tau^* = 0.1$ and 0.2 the velocity $\bar{v}^*$ based on the ergodic distribution (e.g. V.9) is very nearly equal to the velocity $\tilde{v}^*$ based on the uniform distribution. However, at $\tau^* = 0.3$ and 0.4 $\tilde{v}^*$ is substantially less than $\bar{v}^*$. The two velocities are plotted in figure (12).

The character of the crystal deformation obtained is illustrated in figure (13) Assume the hypothetical crystal contains a uniform distribution of dislocations, and, moreover, that the density of these dislocations is independent of temperature and stress. In this case the strain rate ($\dot{\gamma}$) of the crystal is simply proportional to the average glide velocity ($\tilde{v}^*$). Now imagine an experiment in which the crystal is strained by a fixed amount (for example, $\gamma = 0.2$) at a given strain rate (for example, let $\ln v^* = -10$). As illustrated in figure (12) both the stress required to accomplish this deformation and the final appearance of the crystal depend markedly on the temperature at which the experiment is carried out.

As the illustration shows, at relatively low temperature, $\alpha \tilde{=} 260$, a relatively high stress ($\tau^* = 0.4$) is required, and virtually the entire deformation occurs through slip on a single slip plane. At higher temperature, $\alpha \sim 68$, a lower stress is sufficient ($\tau^* = 0.3$), and there is sensible though relatively insignificant slip on planes other than the dominant slip plane. At $\alpha \tilde{=} 35$, $\tau^* = 0.2$ and deformation is reasonably

homogeneous. At $\alpha \sim 22$, $\tau^* = 0.1$ and the deformation is almost perfectly homogeneous.

Hence when the distribution of dislocations is uniform the stress required to carry out the deformation drops as the temperature is raised, and the mode of deformation gradually changes from slip on well-defined slip planes to homogeneous slip. Had we assumed an ergodic distribution of dislocations the required stress would have been higher by an amount which increased with α; however, the mode of deformation would have been homogeneous slip at all values of α.

ACKNOWLEDGEMENT

The authors are grateful to K. L. Hanson and C. K. Syn for helpful discussions. The work reported here was supported by the Atomic Energy Commission through the Inorganic Materials Research Division of the Lawrence Berkeley Laboratory.

REFERENCES

1. J. W. Morris, Jr. and D. H. Klahn, J. Appl. Phys. (in press)
2. J. W. Morris, Jr. and C. K. Syn, J. Appl. Phys. (submitted)
3. A. J. F. Foreman and M. J. Makin, Phil. Mag., 14, 911 (1966)
4. U. F. Kocks, Phil. Mag. 13, 541 (1966)
5. Since completion of the work reported in this paper the code has been thoroughly revised by Kenton Hanson (unpublished). It employs a rather different searching algorithm which is both more efficient than the "circle-rolling" technique and avoids the problems discussed here.
6. U. F. Kocks, Can J. Phys., 45, 737 (1967)
7. J. E. Dorn, P. Guyot, and T. Stefansky, in Physics of Strength and Plasticity, A. S. Argon, ed., MIT Press, Cambridge, Mass. (1969) p. 133.
8. R. L. Fleisher and W. R. Hibbard, in The Relation between the Structure and Mechanical Properties of Metals, H. M. Stationary Office, London, (1963), p. 262.
9. J. Friedel, Dislocations, Addison-Wesley, Reading, Mass (1964), p.224.
10. R. Labusch, Zeit. Phys., 167, 452 (1962)
11. D. H. Klahn and J. W. Morris, Jr., in Rate Processes in Plastic Deformation, J. C. M. Li, ed., Plenum Press (in press).

TABLE I.

The mean transit time and its variance for $\tau^* = 0.4$, $\beta_c = 0.63$, compared with results of three approximations.

		α = 200	α = 300	α = 400
1. Empirical Result: Six Attempts at Each Value of α	$\langle t^* \rangle$	$1.49 \times 10^{4}_{8}$	$1.19 \times 10^{6}_{11}$	$9.57 \times 10^{7}_{15}$
	σ^2	1.21×10^{8}	9.67×10^{11}	4.54×10^{15}
2. Minimum Angle Approximation	$\langle t^* \rangle$	$3.05 \times 10^{4}_{8}$	$2.12 \times 10^{6}_{12}$	$1.64 \times 10^{8}_{15}$
	σ^2	1.64×10^{8}	1.08×10^{12}	7.56×10^{15}
3. Minimum Angle Approximation: Arrenhius Equation	$\langle t^* \rangle$	$7.74 \times 10^{3}_{8}$	$6.97 \times 10^{5}_{11}$	$6.27 \times 10^{7}_{15}$
	σ^2	5.91×10^{8}	4.85×10^{11}	3.93×10^{15}
4. Minimal Sequence Approximation	$\langle t^* \rangle$	$1.87 \times 10^{4}_{7}$	$1.55 \times 10^{6}_{11}$	$1.33 \times 10^{8}_{15}$
	σ^2	6.28×10^{7}	6.27×10^{11}	5.53×10^{15}

FIGURE CAPTIONS

1. Detail of equilibrium in the $i^{\underline{th}}$ configuration.
2. The assumed step form of the dimensionless dislocation-obstacle interaction, $\beta(^{x}/d)$. The obstacle strength is β_c. The shaded area is g_i^k, the dimensionless activation energy required when the dislocation exerts a force β_i^k on the obstacle.
3. The dependence of the strength (β_1) of the most stable configuration on the applied stress, τ^*. The solid bars show the range of values for four arrays. The dashed bars show the range of values for twenty arrays. The solid curve represents the data obtained by Foreman and Makin[3]. The dashed curve is a plot of the Friedel relation (eq. III.1). The insert shows normalized histograms of the β_1 values of 20 arrays at each of three stresses: $\tau^* = 0.1$, 0.3, and 0.5.
4. The most stable configurations found in glide through a typical 999 point array at three stresses: $\tau^* = 0.1$ ($\beta_1 = 0.22$); $\tau^* = 0.3$ ($\beta_1 = 0.44$); and $\tau^* = 0.5$ ($\beta_1 = 0.70$).
5. Normalized histograms of the density of forces (measured as the ratio (β/β_m)) along stable configurations of strength $\beta_m \sim \beta_1$ at each of three stresses: $\tau^*=0.1(\beta_m=0.2339)$; $\tau^*=0.3(\beta_m=0.5080)$; and $\tau^*=0.5(\beta_m=0.7109)$. The method of constructing these histograms is described in the text.
6. The variation of the mean obstacle spacing ($\bar{l}^*$) in the strength-determining configurations with the applied stress (τ^*). The solid circles give the mean value obtained using configurations from 100 randomly chosen arrays at $\tau^* = 0.1$ and 0.3, and configurations from 20 random arrays at $\tau^* = 0.5$. The solid bars show the range of $\bar{l}^*$ for the strength-determining configurations in 20 arrays. The

comparison curves plot the theoretical relations of Friedel[9], Labusch[10], and Kocks [6].

7. Histograms showing the distribution of the strengths (β_i) of the configurations encountered along the minimum angle path (χ_o) at each of three stresses, $\tau^* = 0.1$, 0.3, and 0.5. The histograms were obtained by superimposing data from 20 random arrays. The area under the curves gives the mean number r of stable configurations on χ_o per array, and is r = 890 at $\tau^* = 0.1$, 750 at $\tau^* = 0.3$, and 470 at $\tau^* = 0.5$.

8. Histogram showing the normalized density of forces (β) along the $50^{\underline{th}}$ configuration encountered in glide at $\tau^* = 0.1$. The histogram was found by superimposing data obtained from 200 random arrays.

9. The five strongest configurations encountered in glide through a typical array at $\tau^* = 0.1$. The strengths are: $\beta_1 = 0.2154$, $\beta_2 = 0.2155$, $\beta_3 = 0.2176$, $\beta_4 = 0.2192$, and $\beta_5 = 0.2203$.

10. Results of a simulation of thermally-activated glide, showing the average glide velocity $\langle v^* \rangle$ as a function of the thermal parameter (α) at two stresses: $\tau^* = 0.1$ and $\tau^* = 0.4$, with obstacle strength $\beta_c = 0.63$. The circles show the average of six trials. The bars show the range in $-\ln\langle v^* \rangle$ as the transit time ranges over $\langle t^* \rangle \pm \sqrt{\sigma^2}$. The comparison plots show estimates obtained from the minimum angle approximation (dashed curve) and from an Arrenhius equation based on time required to activate past the strongest obstacle configuration.

11. The cumulative distribution $N(\Lambda)$ of the activation parameter (Λ) at $\tau^* = 0.4$, $\beta_c = 0.63$, and $\alpha = 300$. The dashed curve gives the distri-

bution along the path χ_o; the solid curve is the average of the distributions of the actual paths taken in six trials.

12. Comparison of the velocity-temperature relations for four arrays of 999 obstacles having $\beta_c = 0.63$ at each of four stresses. Also included are the velocity-temperature curves for a crystal made up of these four arrays under each of two assumptions: an ergodic distribution of dislocations over the planes (----) and a uniform distribution of dislocations over the planes (-·-·).

13. Illustration of the deformation of a hypothetical crystal made up of the four glide planes whose properties are shown in figure 12. This figure shows the change in the appearance of the deformed crystal with temperature, assuming that the crystal contains a uniform distribution of dislocations of fixed density, and is given a total shear strain $\gamma = 0.2$ at a fixed strain rate such that $-\ln \tilde{v}^* = 10$.

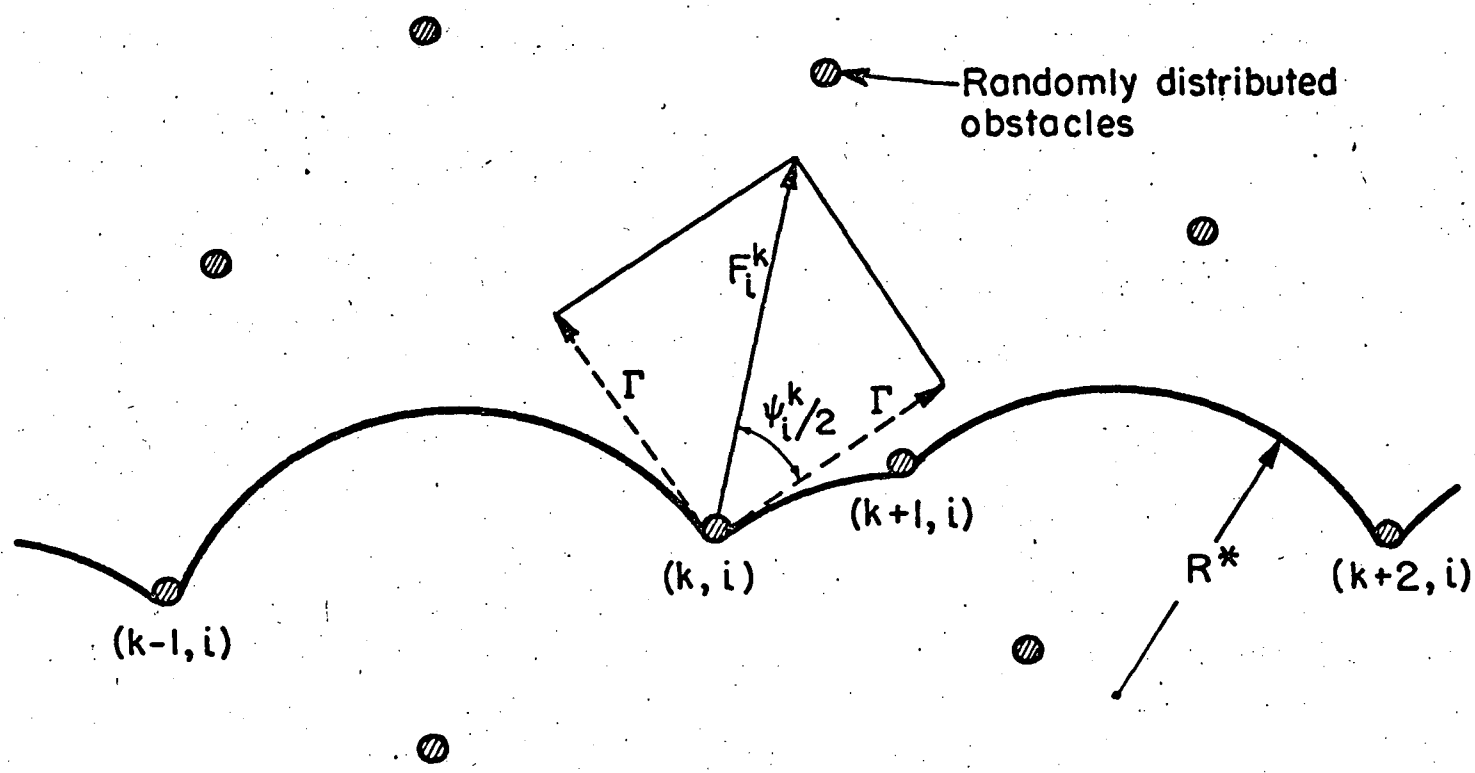
Randomly distributed obstacles
F_i^k
Γ
$\psi_i^k/2$
Γ
(k+1, i)
(k, i)
(k-1, i)
R*
(k+2, i)
XBL732-5721

Fig. 1.

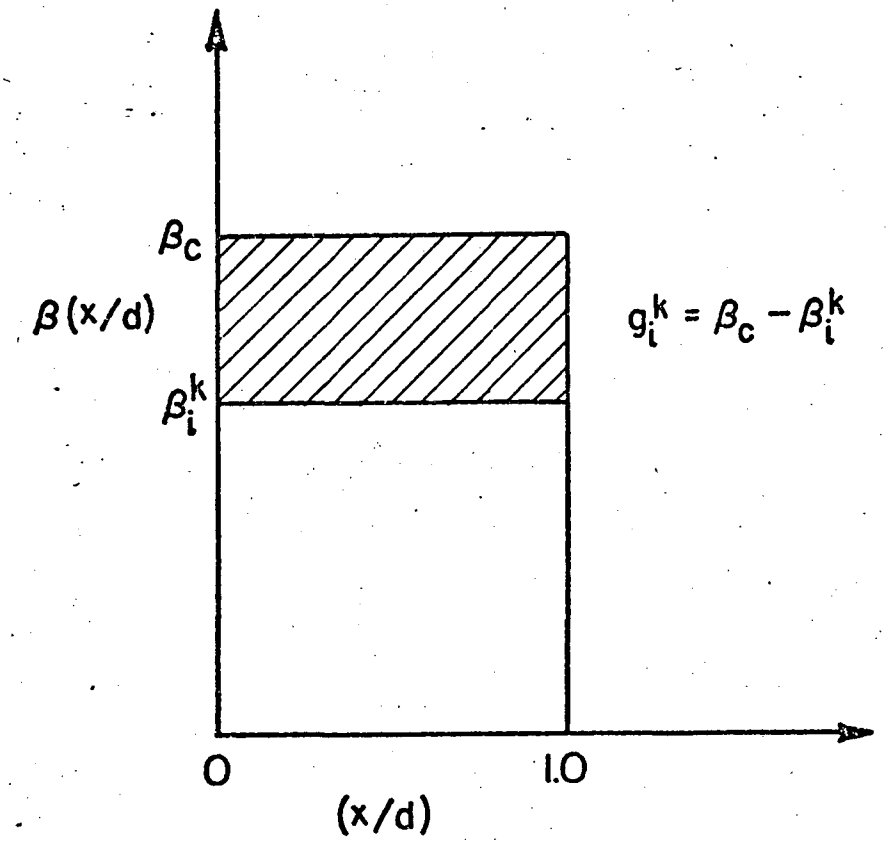

Fig. 2.

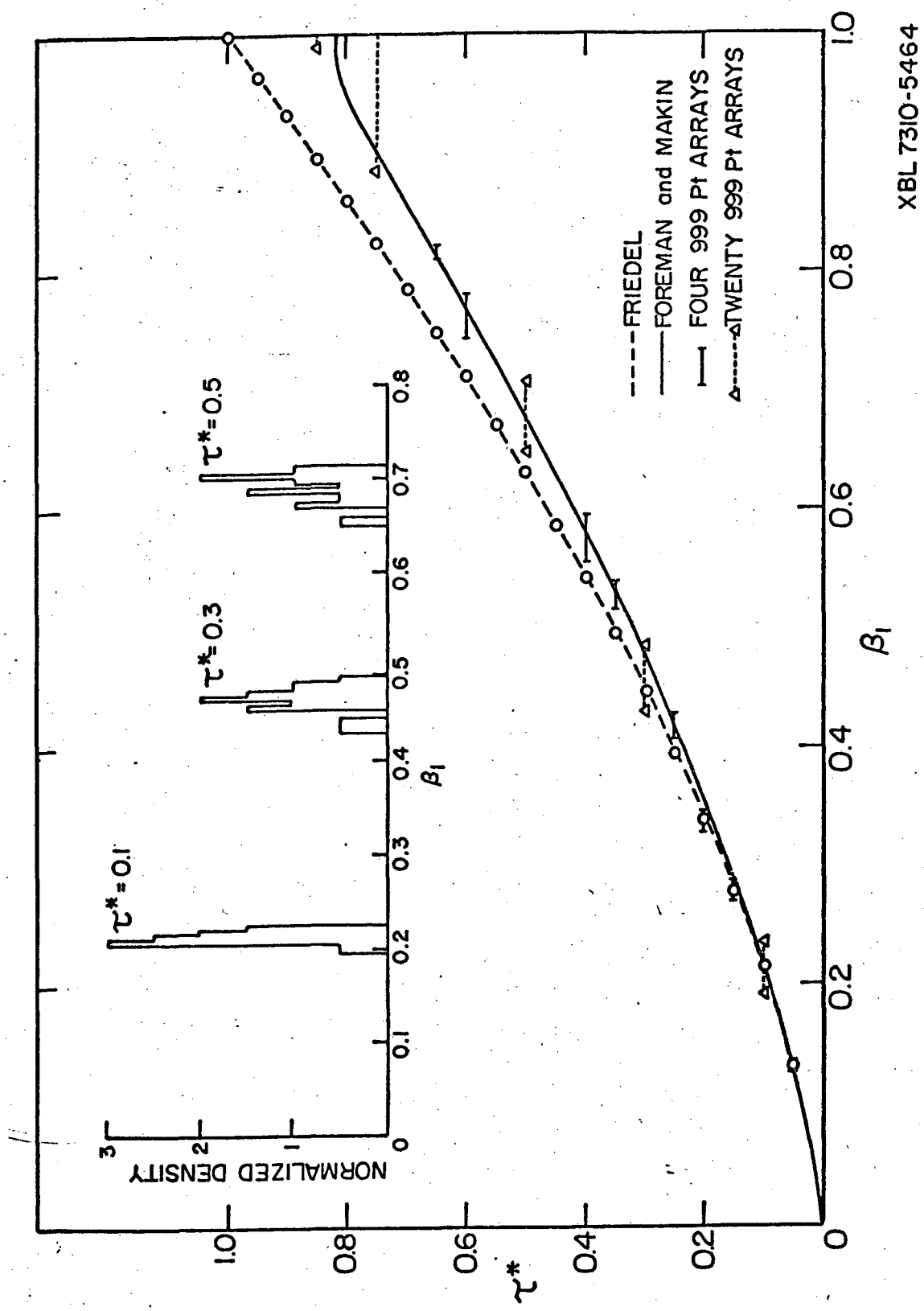
FRIEDEL
FOREMAN and MAKIN
FOUR 999 Pt ARRAYS
TWENTY 999 Pt ARRAYS
τ*
β1
NORMALIZED DENSITY
τ*=0.1
τ*=0.3
τ*=0.5
XBL 7310-5464

Fig. 3.

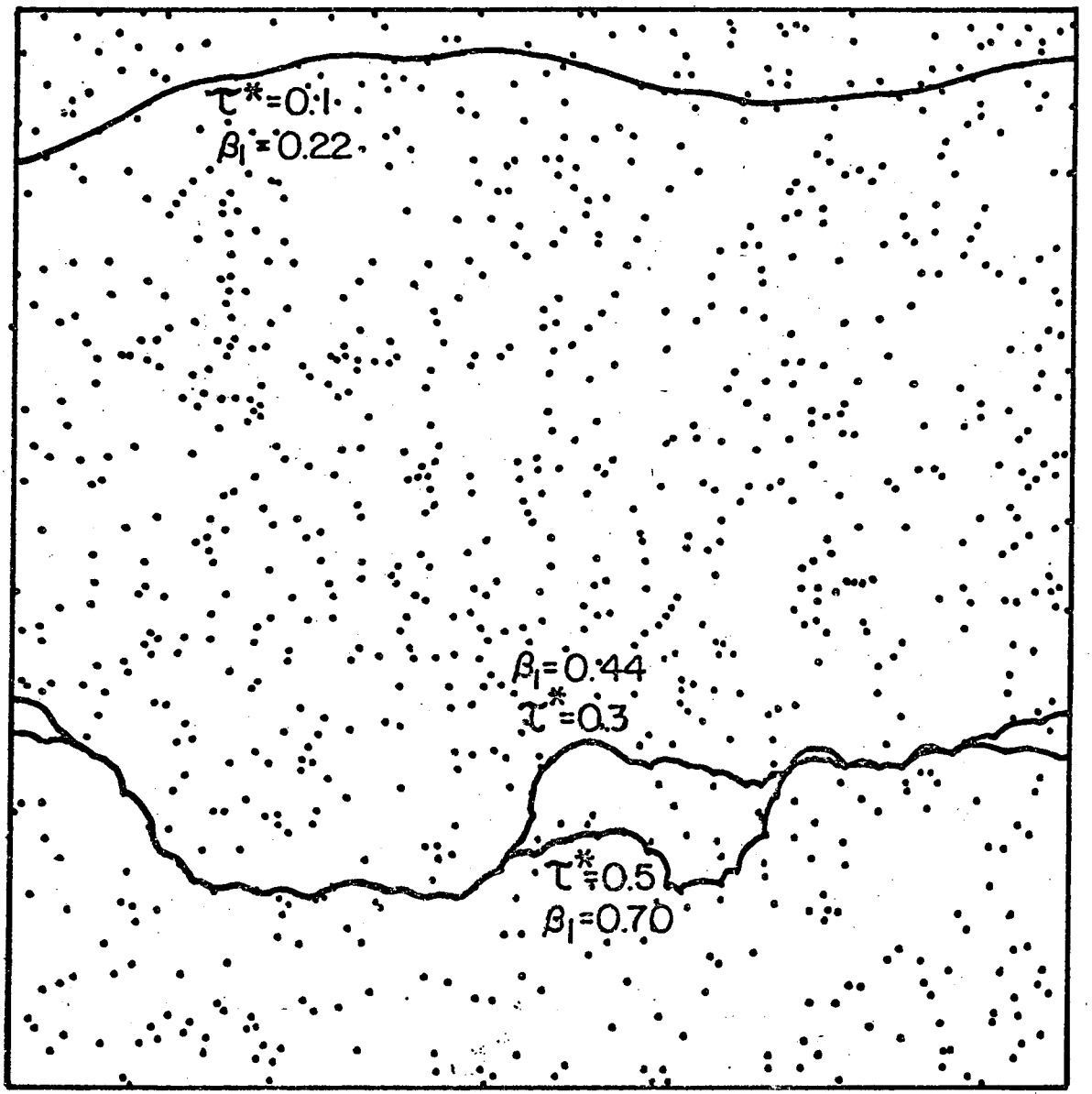

XBL7310-5459

Fig. 4.

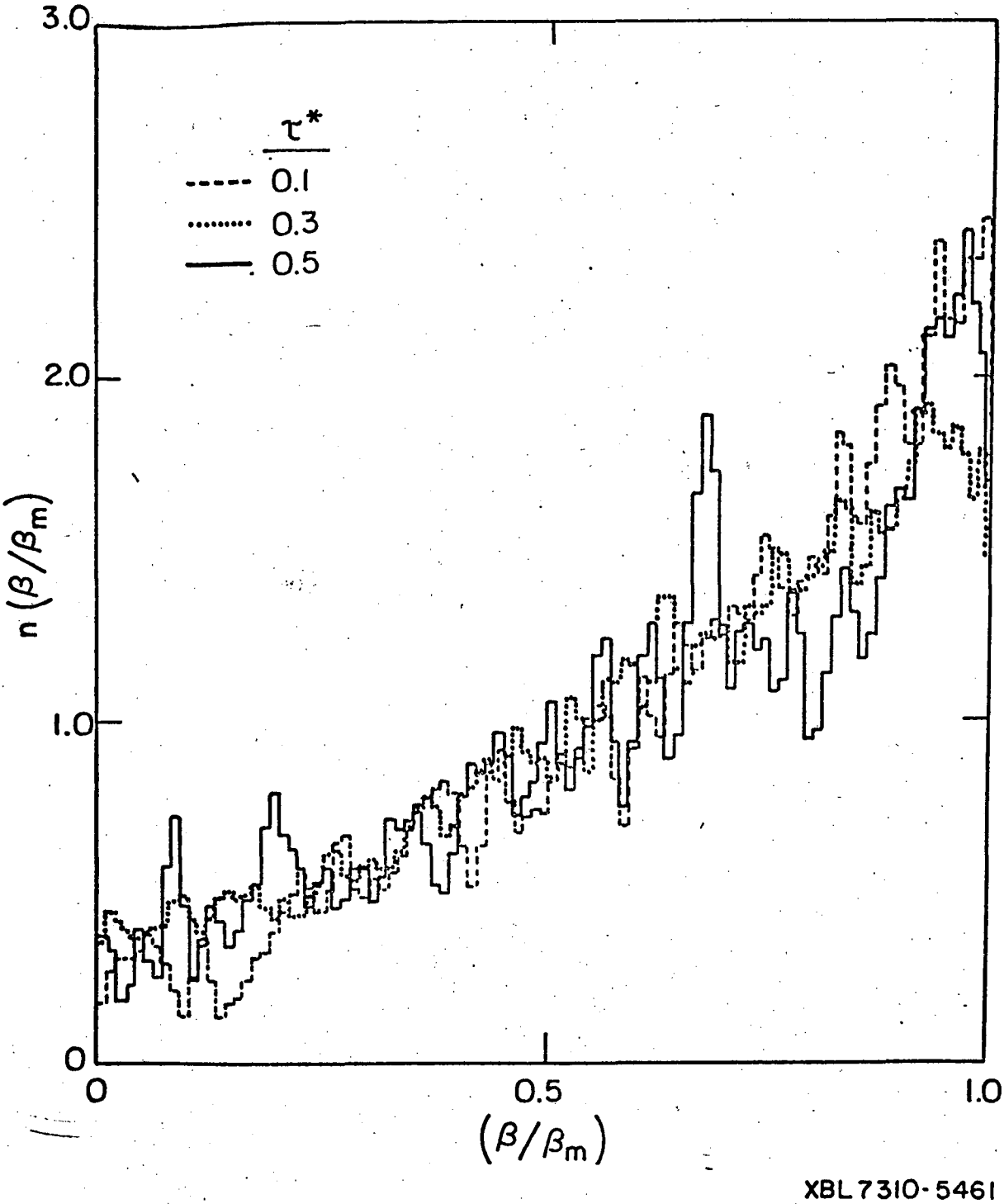
3.0
2.0
1.0
0
0
0.5
1.0
τ^*
0.1
0.3
0.5
$n(\beta/\beta_m)$
(β/β_m)
XBL7310-5461

Fig. 5.

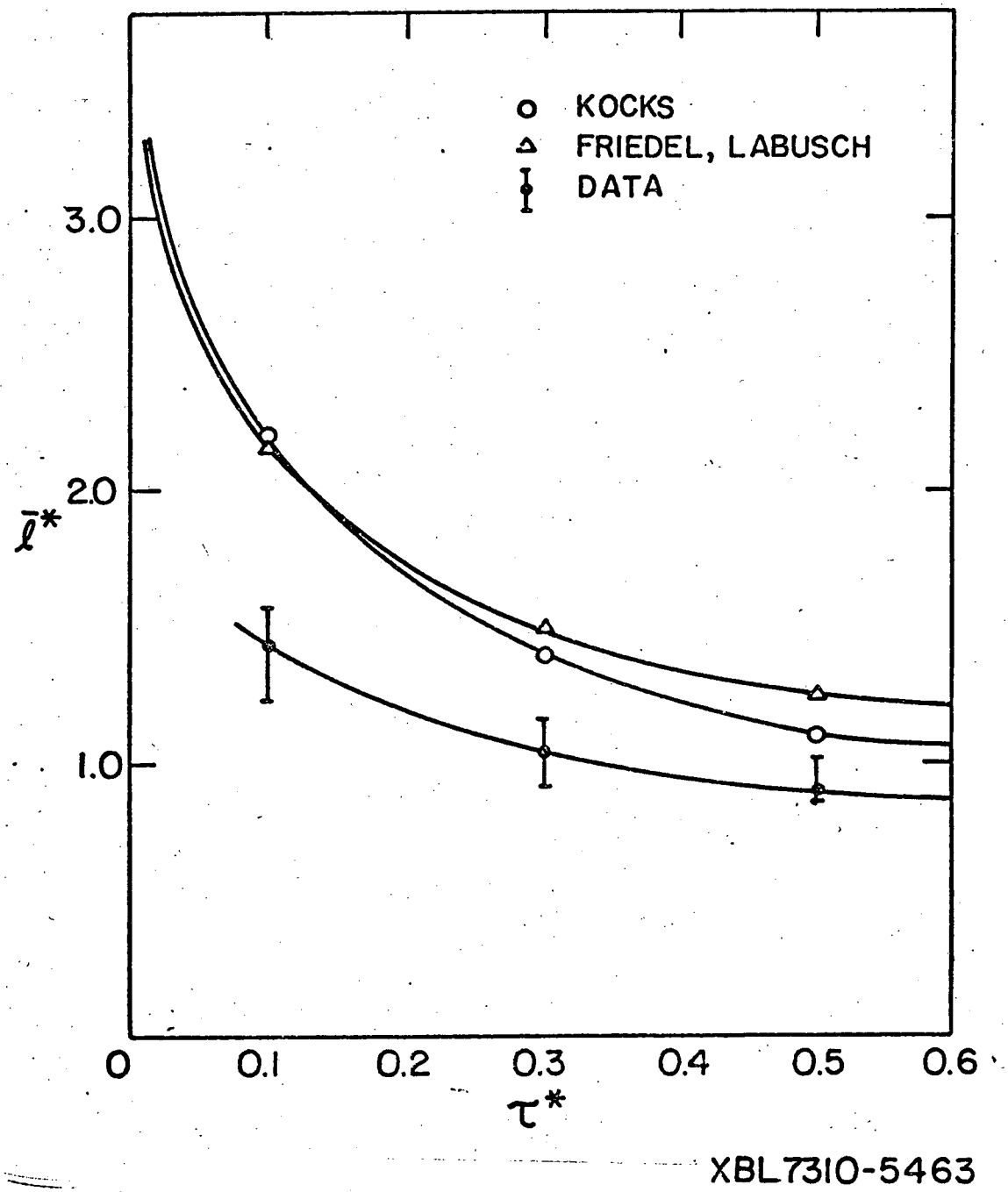
KOCKS
FRIEDEL, LABUSCH
DATA
3.0
2.0
1.0
$\bar{l}^*$
0
0.1
0.2
0.3
0.4
0.5
0.6
τ^*
XBL7310-5463

Fig. 6.

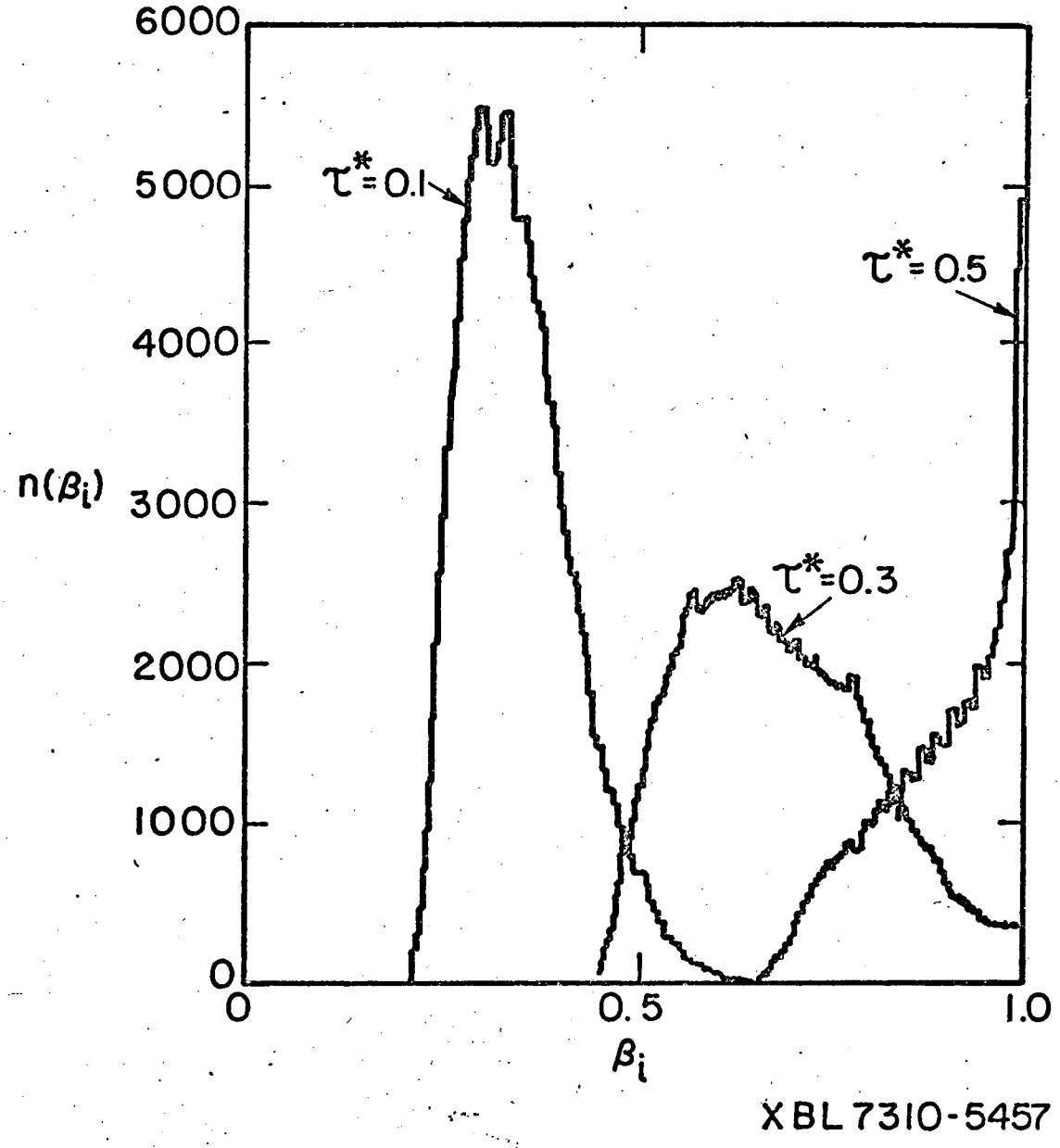
6000
5000
4000
3000
2000
1000
0
n(βi)
τ*=0.1
τ*=0.5
τ*=0.3
0
0.5
1.0
βi
XBL7310-5457

Fig. 7.

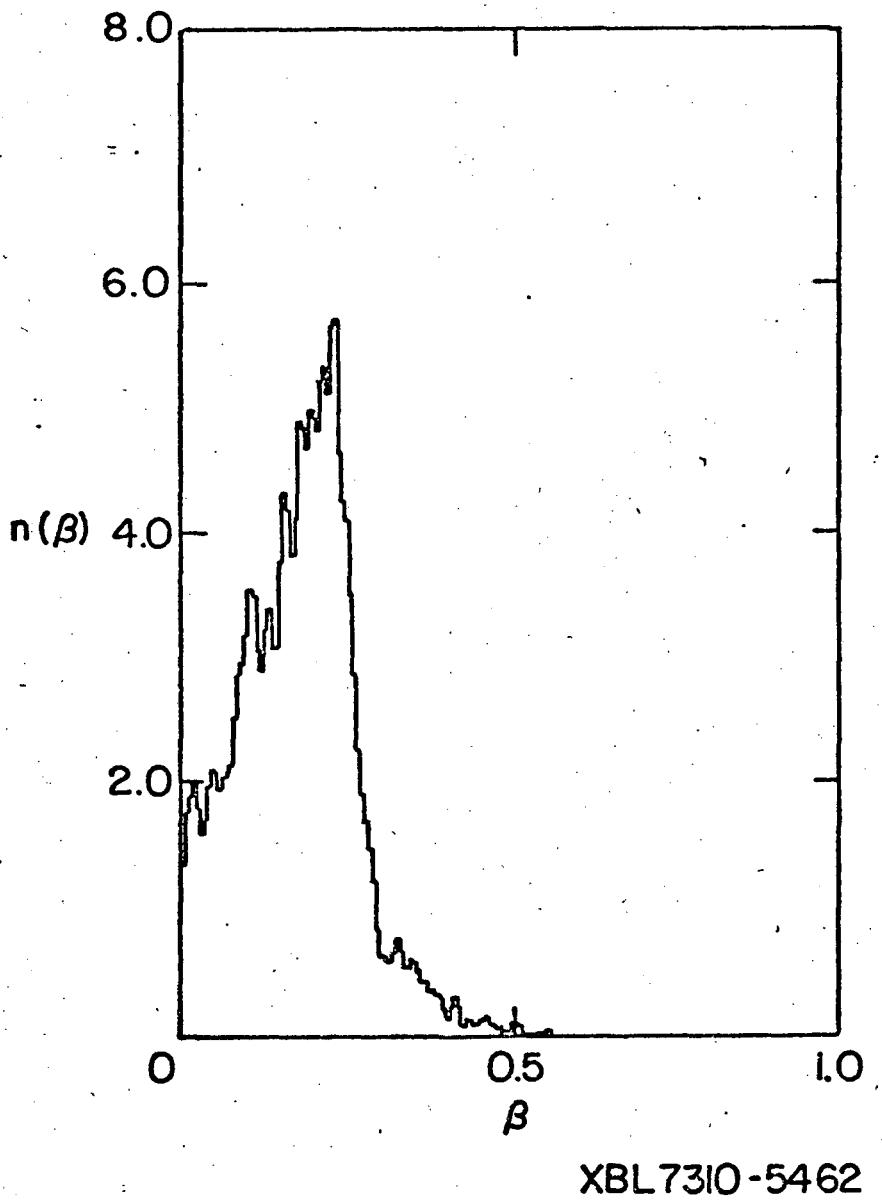

Fig. 8.

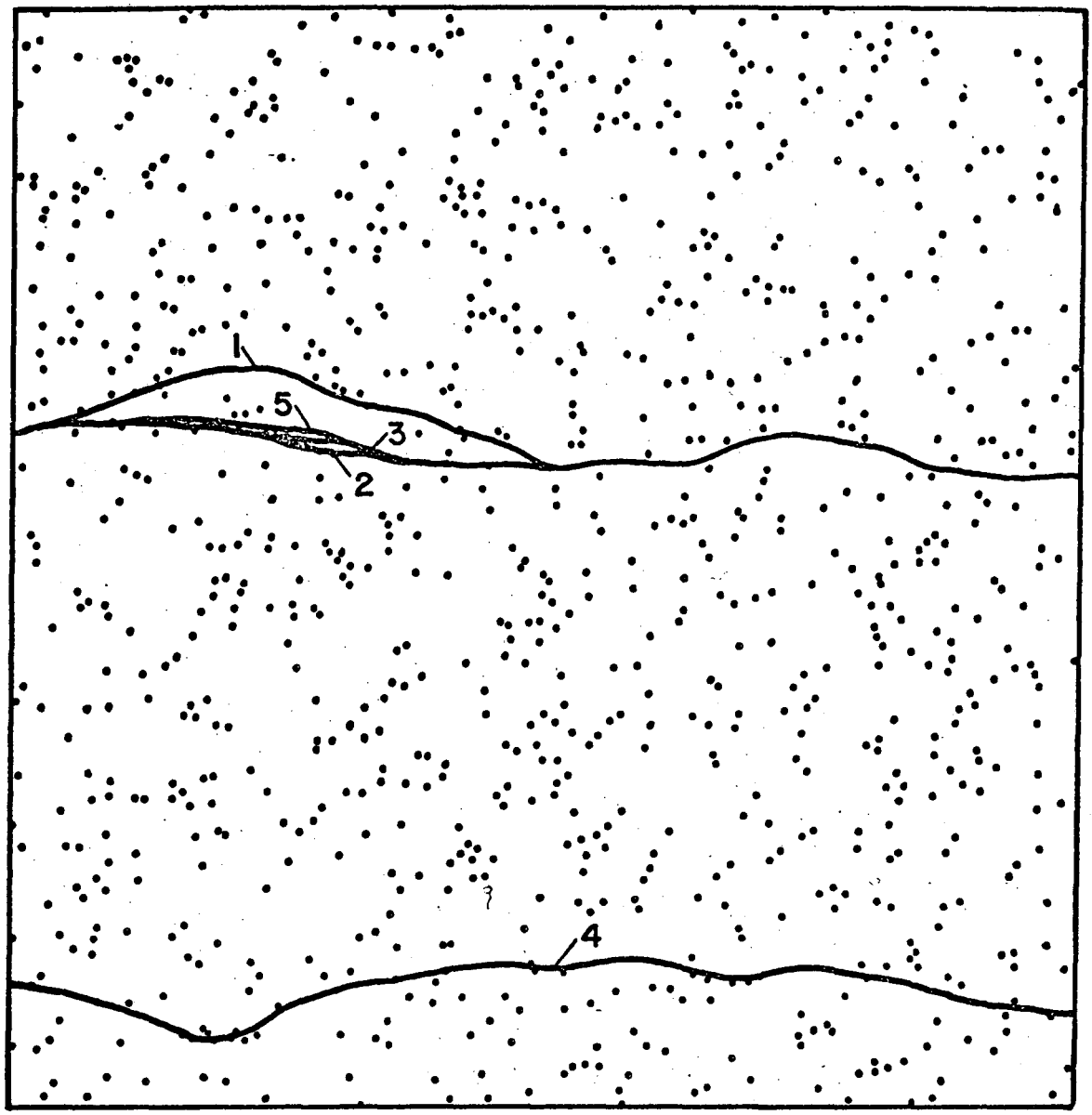

XBL7310-5460

Fig. 9.

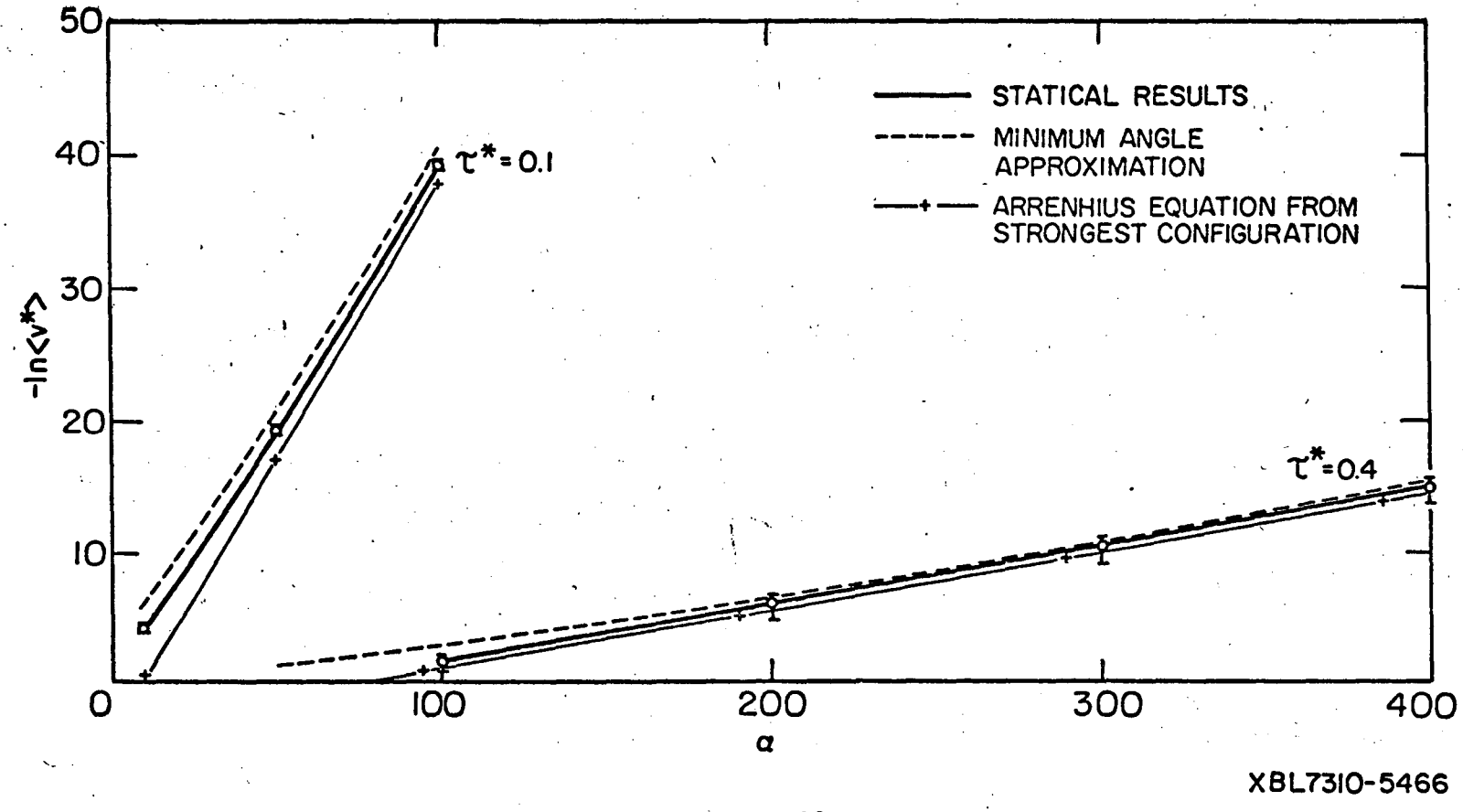
50
40
30
20
10
0
100
200
300
400
α
-ln<v*>
τ*= 0.1
τ*=0.4
STATICAL RESULTS
MINIMUM ANGLE APPROXIMATION
ARRENHIUS EQUATION FROM STRONGEST CONFIGURATION
XBL7310-5466

Fig. 10.

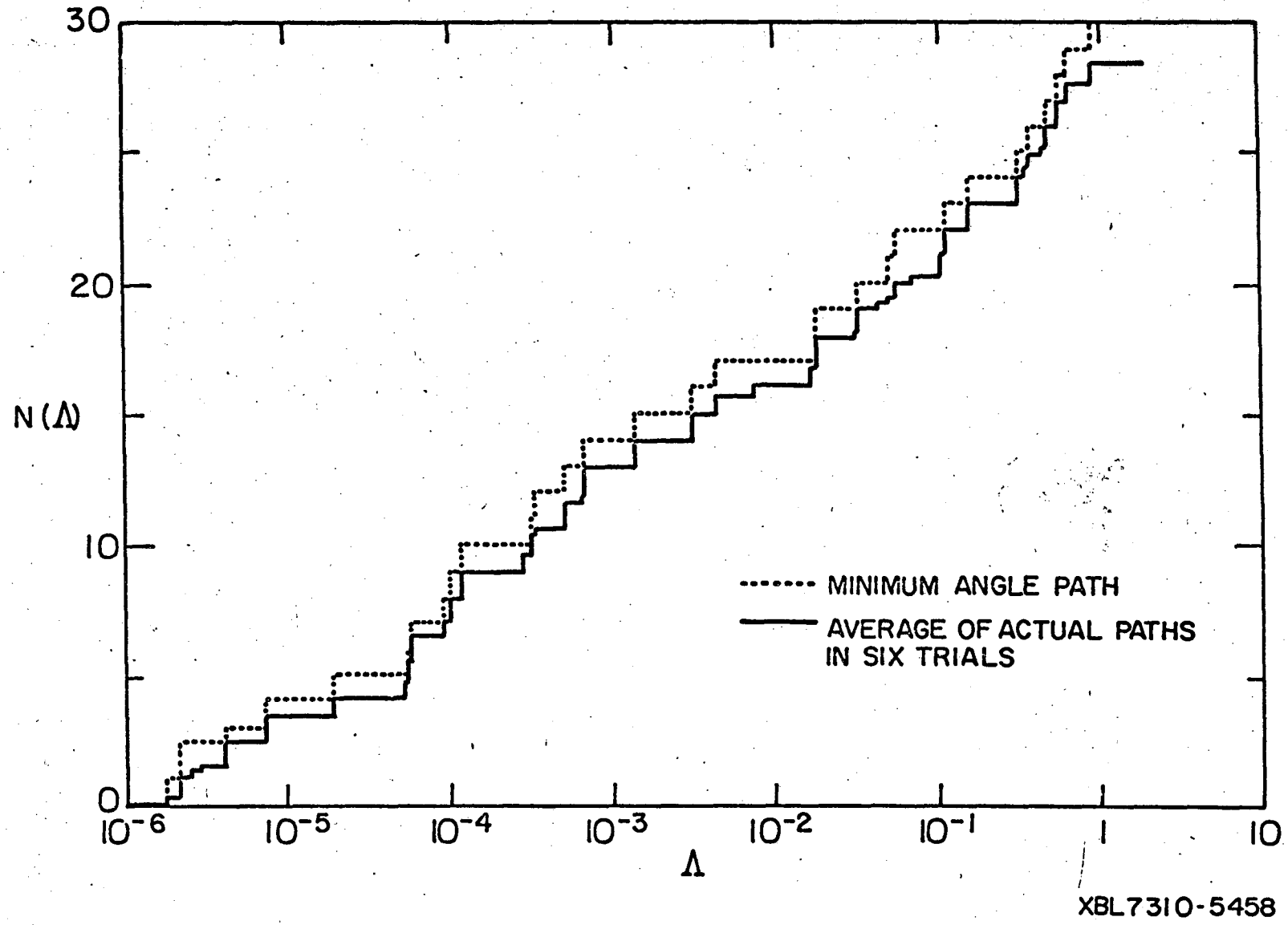
30
20
10
0
N(Λ)
10⁻⁶
10⁻⁵
10⁻⁴
10⁻³
10⁻²
10⁻¹
1
10
Λ
MINIMUM ANGLE PATH
AVERAGE OF ACTUAL PATHS
IN SIX TRIALS
XBL7310-5458

Fig. 11.

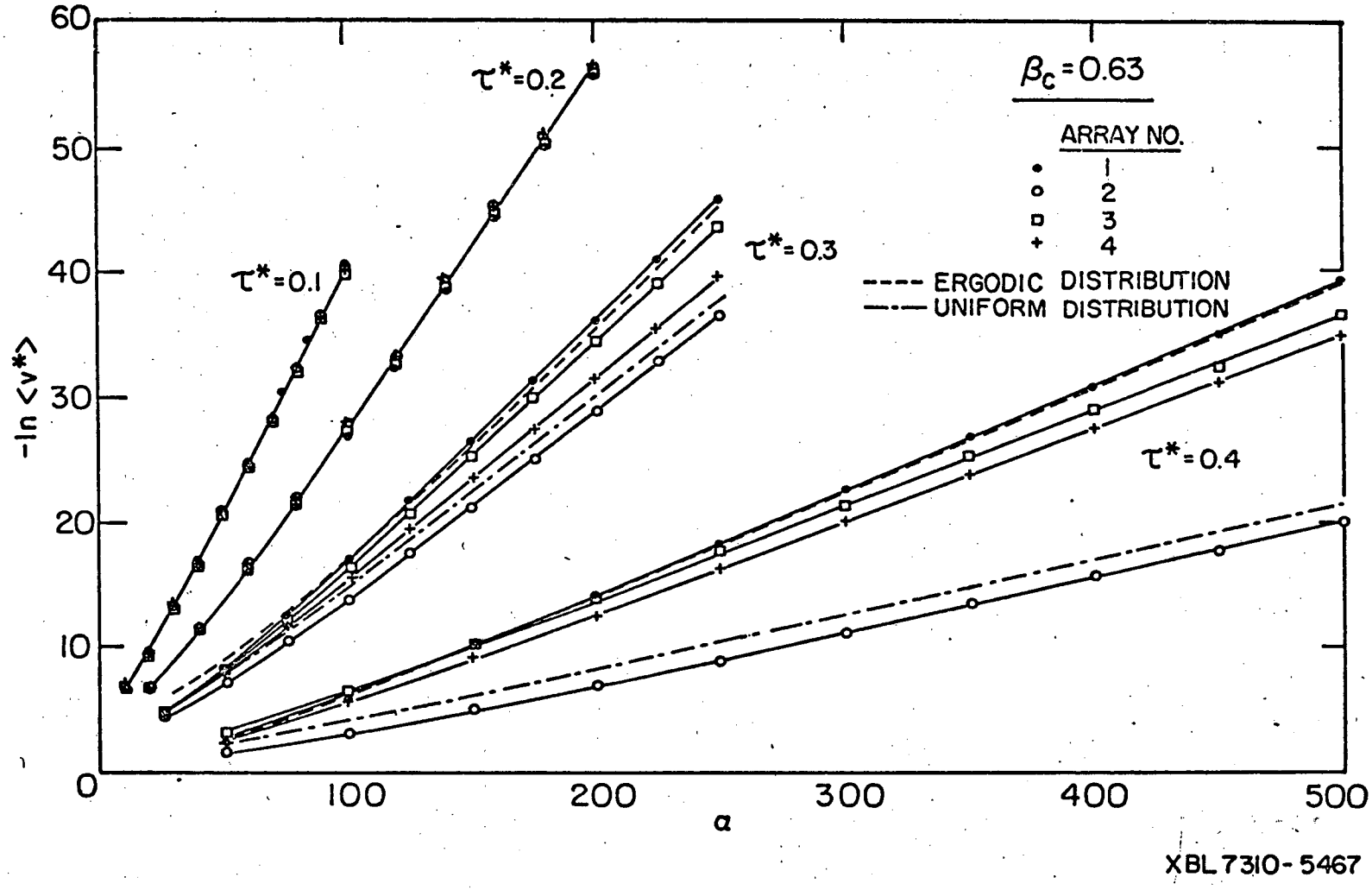
60
50
40
30
20
10
0
100
200
300
400
500
α
-ln <v*>
τ*=0.1
τ*=0.2
τ*=0.3
τ*=0.4
βc=0.63
ARRAY NO.
1
2
3
4
---- ERGODIC DISTRIBUTION
—·— UNIFORM DISTRIBUTION
XBL7310-5467

Fig. 12.

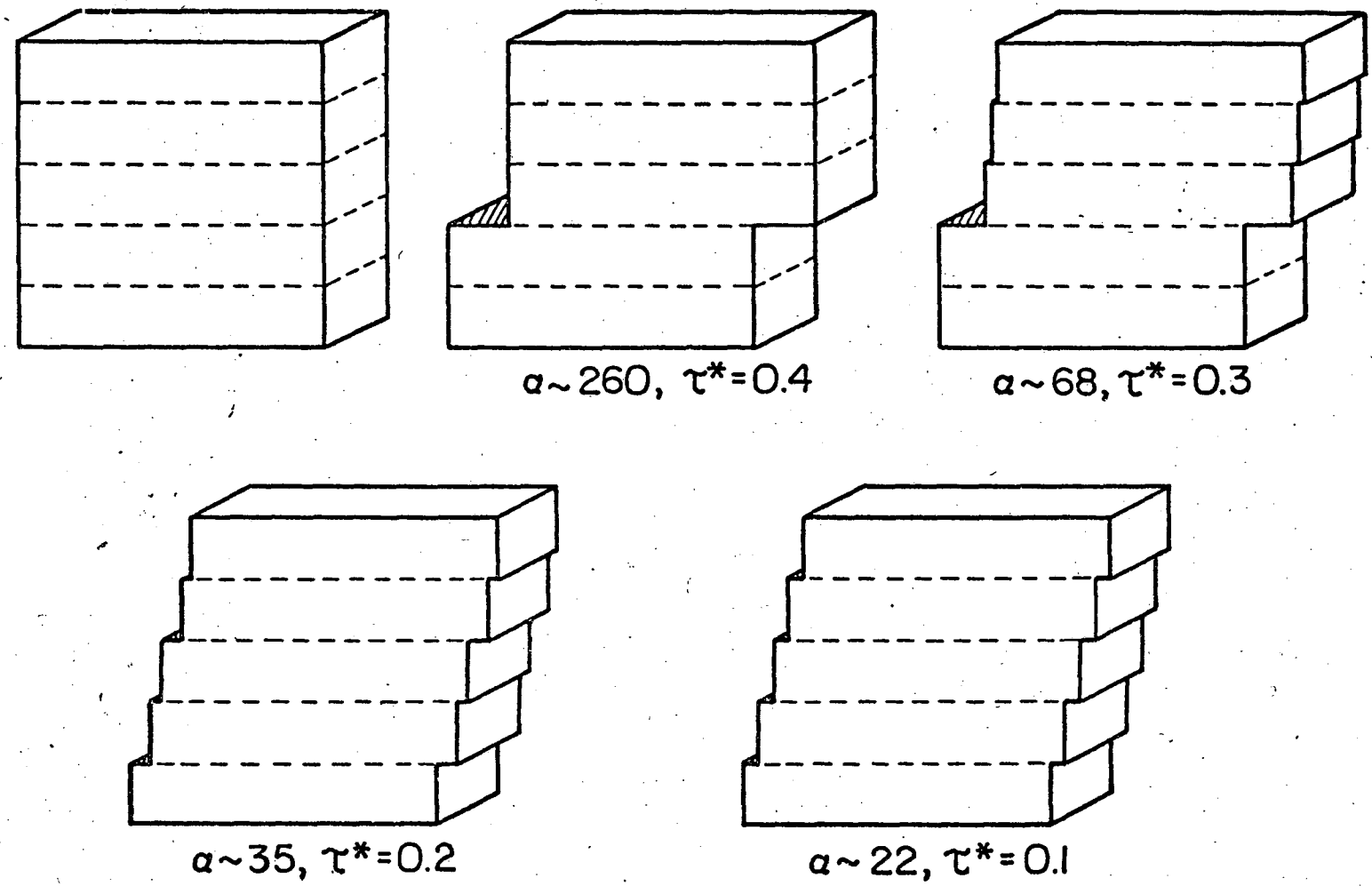

Fig. 13.

TECHNICAL INFORMATION DIVISION
LAWRENCE BERKELEY LABORATORY
UNIVERSITY OF CALIFORNIA
BERKELEY, CALIFORNIA 94720